Journal of Radiation Research, 2015, 56, 239–247
doi: 10.1093/jrr/rru096 Advance Access Publication 31 October 2014

In vivo measurement of dose distribution in patients' lymphocytes: helical tomotherapy versus step-and-shoot IMRT in prostate cancer

Felix ZWICKER[1,2,*], Benedict SWARTMAN[1], Falk ROEDER[1,2], Florian STERZING[1,2], Henrik HAUSWALD[1], Christian THIEKE[1,2], Klaus-Josef WEBER[1], Peter E. HUBER[1,2], Kai SCHUBERT[1], Jürgen DEBUS[1,2] and Klaus HERFARTH[1]

[1]Department of Radiation Oncology, University of Heidelberg, Im Neuenheimer Feld 400, 69120 Heidelberg, Germany
[2]Clinical Cooperation Unit Radiation Oncology, German Cancer Research Center (DKFZ), Heidelberg, Germany
*Corresponding author: Department of Radiation Oncology, University of Heidelberg, Im Neuenheimer Feld 400, 69120 Heidelberg, Germany. Tel: +49-6221-42-2586; Fax: +49-6221-56-5353; Email: f.zwicker@dkfz.de

(Received 7 May 2014; revised 7 September 2014; accepted 13 September 2014)

In radiotherapy, *in vivo* measurement of dose distribution within patients' lymphocytes can be performed by detecting gamma-H2AX foci in lymphocyte nuclei. This method can help in determining the whole-body dose. Options for risk estimations for toxicities in normal tissue and for the incidence of secondary malignancy are still under debate. In this investigation, helical tomotherapy (TOMO) is compared with step-and-shoot IMRT (SSIMRT) of the prostate gland by measuring the dose distribution within patients' lymphocytes. In this prospective study, blood was taken from 20 patients before and 10 min after their first irradiation fraction for each technique. The isolated leukocytes were fixed 2 h after radiation. DNA double-stranded breaks in lymphocyte nuclei were stained immunocytochemically using anti-gamma-H2AX antibodies. Gamma-H2AX foci distribution in lymphocytes was determined for each patient. Using a calibration line, dose distributions in patients' lymphocytes were determined by studying the gamma-H2AX foci distribution, and these data were used to generate a cumulative dose–lymphocyte histogram (DLH). Measured *in vivo* (DLH), significantly fewer lymphocytes indicated low-dose exposure (<40% of the applied dose) during TOMO compared with SSIMRT. The dose exposure range, between 45 and 100%, was equal with both radiation techniques. The mean number of gamma-H2AX foci per lymphocyte was significantly lower in the TOMO group compared with the SSIMRT group. In radiotherapy of the prostate gland, TOMO generates a smaller fraction of patients' lymphocytes with low-dose exposure relative to the whole body compared with SSIMRT. Differences in the constructional buildup of the different linear accelerator systems, e.g. the flattening filter, may be the cause thereof. The influence of these methods on the incidence of secondary malignancy should be investigated in further studies.

Keywords: dose distribution; helical IMRT; lymphocytes; *in vivo* dosimetry; gamma-H2AX; tomotherapy; step-and-shoot IMRT; prostate cancer

INTRODUCTION

Reduction of dose in organs at risk and healthy tissue is an important field of radiation research. Ideally, this can be achieved without impairing the dose being delivered to a tumor with high conformity.

Variations in irradiation techniques lead to differences in dose distribution [1]. Recently, we developed an approach for *in vivo* measurement of the dose distribution within a patients's lymphocytes relative to the whole body. This approach is based on the detection of gamma-H2AX foci in lymphocyte nuclei [2], and it could be useful in estimating the degree of biological dose effect relative to the whole body volume. It is based on the following strategy.

A well-established method for detecting DNA double-strand breaks (DSBs) in human lymphocytes is the gamma-H2AX stain [3]. H2AX-histones at or near irradiation-induced DSBs are phosphorylated, sensitively indicating the presence of DSB repair. Thus DSBs can be visualized indirectly by immunocytochemical staining of the gamma-H2AX foci using a fluorescence microscope [4, 5]. Since DSB induction increases linearly with the delivered dose, the number of

gamma-H2AX foci can be utilized as a reliable parameter for estimating the delivered dose [6]. These irradiation-induced cellular responses are equally efficient at a range of dose levels, but it is evident that a certain level of DNA damage is necessary to activate DNA repair (~1 mGy) [7]. Gamma-H2AX foci are an indirect marker, and their numerical equality with the exact number of DSBs, especially after repair, is currently under debate [8, 9]. In the human body, lymphocytes are convenient biological dosimeters because they can easily be taken from a peripheral vein.

This new method of biological dosimetry can serve as a surrogate for dose distribution in the irradiated body volume. The limitations of this method, e.g. circulation of the lymphocytes in the body during irradiation [6], have previously been critically discussed [2].

Prostate cancer is a frequent malignant tumor and a typical malignancy that is regularly treated with radiotherapy, resulting in long-term patient survival [10, 11]. The use of radiotherapy in locally limited prostate cancer is increasing compared with surgical techniques. Both methods are seen as comparable in terms of local control and long-term survival.

In order to minimize normal tissue dosage, conformal techniques, including intensity-modulated radiotherapy (IMRT), have become standard in the irradiation treatment of prostate cancer [12, 13].

Using the methodology of *in vivo* measurement of the dose distribution within patients' lymphocytes, our group has recently demonstrated in prostate cancer that lymphocytes indicated a significantly decreased middle-dose exposure during SSIMRT compared with during conventional 3D-conformal radiotherapy [2].

A relatively new method in intensity-modulated radiotherapy is helical tomotherapy (TOMO). The technical details of TOMO have been discussed in detail previously [14]. Essentially, a TOMO unit is a hybrid of a 6-MV linear accelerator and a helical CT scanner. Treatment is administered using a rotating fan beam, and as the patient is moved through the gantry bore, the treatment beam forms a helix [14, 15]. The beam is modulated by a very fast-moving, pneumatically driven, binary multileaf collimator (MLC). In an inverse treatment-planning process, the MLC conformation is optimized to obtain highly conformal radiation doses at the target [16].

Because tomotherapy is increasingly used for radiotherapy for prostate cancer, we present our data using this *in vivo* radiation dosimetry approach, comparing helical IMRT/tomotherapy (TOMO) and SSIMRT. Our results suggest that TOMO may have advantages with respect to low-dose radiation distributions, at least in the context of the current linac equipment.

MATERIALS AND METHODS

Patients and irradiation

Individuals of both groups were treated and investigated in the same period (2009–2010) within a prospective study. All patients exhibited prostate cancer saved by biopsy and had an indication for irradiation of the prostate gland.

The study was approved by the Ethics Committee of the University Hospital of Heidelberg. All patients gave their informed consent.

Exclusion criteria were prior radiation in the patient's medical history or additional radiation of lymphatic pelvic regions. A total of 20 patients were recruited for each treatment method (SSIMRT, TOMO); see Fig. 1. Patients' treatment was not influenced by the study, and attribution to the different modalities was made coincidentally in the clinical daily routine, as it was quasi-randomized. Definitions of CTV and PTV for all patients were performed identically, according to the institute's guidelines. For treatment planning, CT scans were performed with 3-mm slice thickness at full bladder and empty rectum. The PTV comprised the prostate gland, seminal vesicles (including the bottom of the bladder) and the anterior rectal wall,

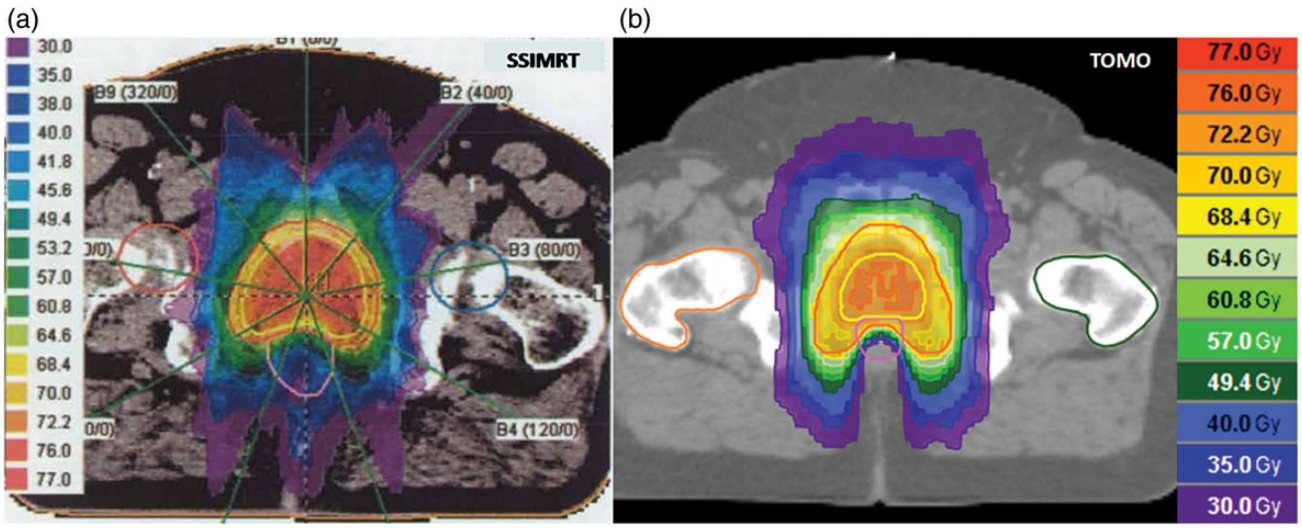

Fig. 1. Examples of dose distribution in radiotherapy of the prostate gland with (**a**) SSIMRT and (**b**) TOMO.

Table 1. Patient data

	age (years)	body volume (l)	PTV (cm^3)
SSIMRT	71.6 (65.4–81.9)	85.4 (53.8–103.2)	181.0 (71.8–337.1)
TOMO	69.9 (54.9–78.8)	86.5 (63.4–107.5)	153.4 (104.1–202.9)

The median values (with range) are shown. The body volume (l) was calculated as body weight (kg) × 1.075 l/kg.

with a margin of 0.5 cm dorsally and 0.8 cm in other directions. The anterior rectal wall (one-third of the total circumference) did not exceed more than 70 Gy in median.

Clinical follow-up was carried out according to the national guidelines including clinical investigation and PSA controls carried out by the patient's attending urologic doctor. Patients of the SSIMRT and TOMO groups demonstrated a very distinct reduction of the PSA value 3–12 months after the end of radiotherapy, with the exception of two patients (SSIMRT) with distant metastases in the follow-up. Side effects > Grade 3 (RTOG) were not described.

Inverse treatment planning was performed using the KonRad software developed at the German Cancer Research Center (DKFZ). The planning process for IMRT treatment has been described in detail previously [17]. Inverse planning for regular TOMO delivery was performed with the Tomotherapy planning software. Further patient data comparing SSIMRT with TOMO are shown in Table 1.

Radiotherapy was performed using the Department's linear accelerators: (i) Oncor (Siemens/Germany) for SSIMRT and (ii) Tomotherapy Hi-Art (Accuray/USA) for helical-IMRT (TOMO). Technical parameters of the different radiation modalities are presented in Table 2.

A calibration line was generated from *ex vivo* irradiation of the blood of five volunteers to calibrate absolute doses to the investigated number of gamma-H2AX foci; see Zwicker *et al*. [2]. The previous calibration curve that was published in [2] shows the slope $y = 7.86 \times \text{dose}$, ($y$ = number of gamma-H2AX foci per nucleus, x = dose in Gy).

Experiments, treatments and analyses of both groups and the calibration line were performed in the same period and at our institute.

Lymphocyte separation and immunofluorescence analysis

For intermixture of irradiated with non-irradiated lymphocytes, blood circulation was given 10 min after the end of the first treatment fraction until the patients's blood (7.5 ml) was taken from a peripheral vein. Negative controls were also taken from each patient before irradiation treatment. All samples were coded to prevent bias during manual scoring.

Gamma-H2AX foci in lymphocyte nuclei were stained by indirect immunofluorescence. This validated method for detecting DNA DSBs has been published in numerous papers [18, 19, 20].

Table 2. Technical data: SSIMRT vs TOMO

	SSIMRT	TOMO
Beams	7–9	helical
Energy (MV)	6	6
SD (Gy)	2.17	2.17
CD (Gy)	76	76
Boost	integrated	integrated
Dose output (Gy/min)	2	8.7
Mean beam-on time (min)	6.2	7.8
Mean table time (min)	16.3	15.5

SD = Single fraction dose, CD = Cumulative dose, MV = Megavolts.

Separating of the lymphocytes from the blood was performed by layering 5 ml of heparinized venous blood onto 3 ml of Ficoll and centrifuging at 2300 rpm for 20 min at 37°C. Then lymphocytes were washed in PBS (6 ml) and centrifuged at 1500 rpm for 10 min (37°C). The generated cell pellet was resuspended at a 1:15 dilution after the buffer was aspirated (room temperature). Approximately 300 000 lymphocytes, diluted in 200 µl, were spread onto a clean slide by means of the Cytospine Centrifuge at 22 rpm for 4 min (room temperature).

Then the lymphocytes were fixed using fixation buffer (3% paraformaldehyde, 2% sucrose in PBS) for 10 min at room temperature. The fixation step was performed 2 h after the end of the first radiation fraction to allow comparability between the samples for all experiments (patients and volunteers for calibration line). Subsequently, cells were permeabilized for 4 min at 4°C (permeabilization buffer: 20 mM HEPES (pH 7.4), 50 mM NaCl, 3 mM $MgCl_2$, 300 mM sucrose and 0.5% Triton X-100). Afterwards, lymphocytes were incubated with anti-gamma-H2AX antibody (Anti-Phospho-Histone-gamma-H2AX Monoclonal IgG-mouse-Antibody (#05-636), Upstate, Charlottesville, VA) at a 1:500 dilution for 1 h (37°C), washed in PBS four times, and incubated with the secondary antibody (Fluorescein-isothiocyanate (FITC)-conjugate, Alexa Fluor 488 Goat-anti-mouse-IgG-conjugate, Molecular Probes, Eugene, OR) at a dilution of 1:200 for 0.5 h (37°C).

Then lymphocytes were washed in PBS (4×, 20°C). To correlate the gamma-H2AX foci with the nuclei, lymphocytes were mounted with VECTASHIELD mounting medium, including the nuclear stain DAPI (Vector Laboratories).

Lymphocytes on the slides were examined with a ×100 objective (fluorescence microscope Laborlux S, Leica Microsystems CMS GmbH, Wetzlar, Germany). Immunofluorescence spots of nuclei were counted by eye because that enabled focusing manually through the whole nucleus with the microscope, thus detecting each focus in the 3D space. Only one trained person counted the gamma-H2AX foci for all the experiments. Within each patient sample (with a heterogeneous dose-distribution), 300 lymphocytes were analyzed. All nuclei were morphologically considered by eye (cell form and size).

Control samples before the first irradiation fraction and *in vitro* samples were analyzed by counting 50 cells for each measuring point and experiment due to their homogenous radiation. Three independent experiments were executed in *in vitro* experiments.

Data and statistical analysis

Gamma-H2AX foci of the lymphocytes were counted for every patient. The averaged relative number of cells was calculated from 20 patients per group (SSIMRT and TOMO) for every count of gamma-H2AX foci per nucleus.

The calibration graph contained lymphocytes of five subjects irradiated *ex vivo* at six different doses (0, 0.02, 0.1, 0.5, 1 and 2 Gy). For each measuring point, three independent experiments were performed.

Due to their homogenous radiation, the *in vitro* samples were investigated by counting 50 cells for each experiment and each measuring point. Background foci levels were subtracted.

The relationship between dose application and irradiation-induced gamma-H2AX foci formation is linear [4]. Thus, we generated a linear regression curve (please see Zwicker *et al*. [2]).

Equivalent absolute doses for every count of irradiation-induced gamma-H2AX foci per nucleus in a patient's lymphocytes were calculated by generated linear regression curve, whereas background foci (controls before irradiation) were subtracted again.

Next, values of gamma-H2AX foci were converted into relative doses related to the prescribed dose (100% corresponds to the given 2.17 Gy in the SSIMRT and TOMO groups). Irrespective of body site or blood flow, this calibration concerns only a single lymphocyte. In addition, we generated a further integral diagram, in which the relative number of lymphocytes with gamma-H2AX foci was plotted against the relative applied dose as a percentage (dose–lymphocyte-histogram/DLH).

The statistics were performed in Sigma.Plot.10.0®. Student's *t*-test with a P-value < 0.05 was defined as significant.

RESULTS

In vivo measurements of patients' lymphocytes

For the investigated lymphocytes of 20 patients per group, the mean numbers of gamma-H2AX foci per nucleus were 0.47 (SSIMRT) and 0.24 (TOMO) ($P < 0.05$) in the irradiated samples (Fig. 2), whereas the non-irradiated controls scored 0.037 gamma-H2AX foci per nucleus on average ($P < 0.05$).

Putting the average *in vivo* foci counts for SSIMRT and TOMO into the calibration curve described above ($y = 7.86x$) [2], the estimated mean biological dose per lymphocyte relative to the whole body is 5.51 cGy in the SSIMRT group and 2.58 cGy in the TOMO group.

Distribution of gamma-H2AX foci

The mean number of lymphocytes with <7 gamma-H2AX foci per nucleus on average was significantly lower in the TOMO than in the SSIMRT group. The mean number of lymphocytes with 7–16 gamma-H2AX foci per nucleus on average was not significantly different between the groups. Lymphocytes with more than 16 gamma-H2AX foci per nucleus were not detected in the TOMO group (Fig. 3).

Dose–lymphocyte histogram

The DLH is a cumulative histogram; each point shows the accumulated number of lymphocytes that has been exposed to at least a certain dose (Fig. 4). Background foci levels have been subtracted because they were also subtracted in the calibration line. The two groups were compared by

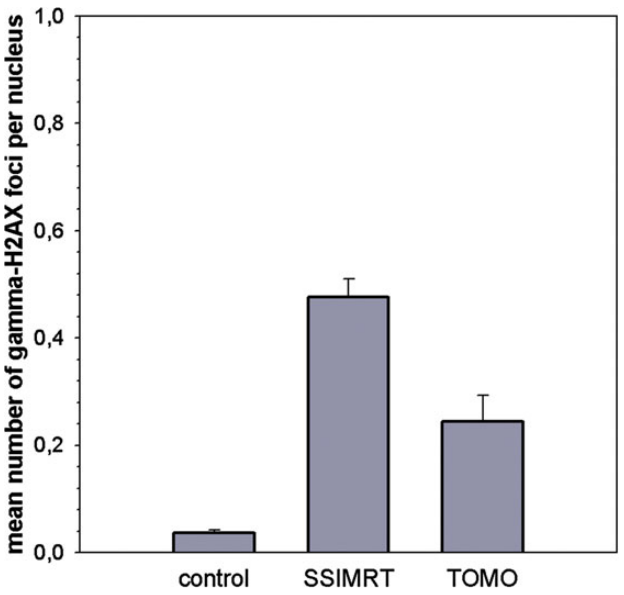

Fig. 2. The average of mean number of gamma-H2AX foci per nucleus in irradiated lymphocytes and negative controls of 20 patients per group is shown (SSIMRT and TOMO). Standard errors are shown. All patients were irradiated in the prostate region, and venous blood was taken before (control) and 10 min after their first irradiation fraction. Lymphocytes were fixed 2 h after the end of the irradiation. In the negative control, 50 lymphocytes were analyzed per patient; in the irradiated samples, 300 lymphocytes were analyzed per patient.

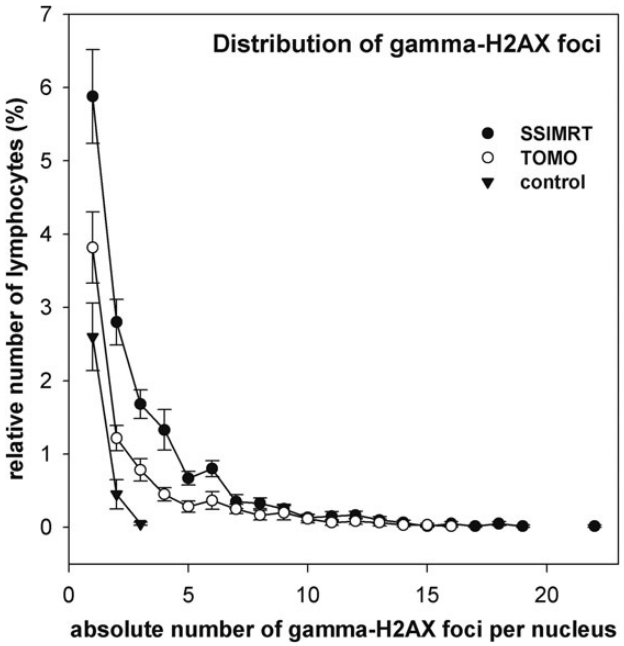

Fig. 3. Distribution of gamma-H2AX foci in patients' lymphocytes. Data from 20 patients per group (SSIMRT and TOMO) are summarized in two curves. Standard errors are shown.

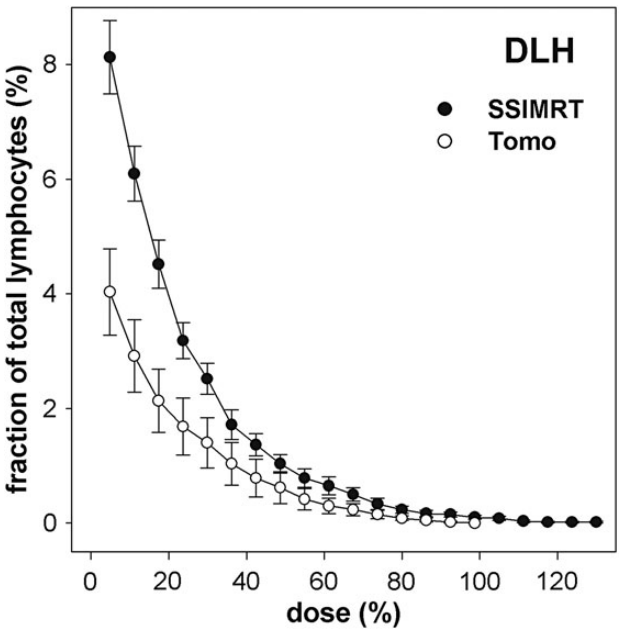

Fig. 4. Dose–lymphocyte histogram (DLH). In this integral histogram, data from 20 patients per group (SSIMRT and TOMO) are summarized in two curves. Standard errors are shown. Initially irradiation dose was correlated with each number of γH2AX foci. Background foci levels were subtracted. Referring to a previously generated calibration line (see Materials and Methods and [2]), the count of γH2AX foci leads to the equivalent delivered dose for each lymphocyte. Each point represents the mean relative sum of lymphocytes with at least the indicated relative dose (≥*x*). A dose of 100% is equivalent to 2.17 Gy for SSIMRT and TOMO.

performing *t*-tests for each individual pair of datapoints along the curves. At dose levels lower than 40% of the described dose, the TOMO curve lies significantly below the SSIMRT curve ($P \le 0.05$). There is no significant difference in the relative number of lymphocytes between 45 and 100% of the applied dose. In comparison with the SSIMRT group, lymphocytes of the TOMO group do not show dose exposure above 100% of the described dose.

The percentage of lymphocytes exposed to more than 50% of the prescribed dose is 0.9% in the SSIMRT group and 0.5% in the TOMO group.

Analyses of dose–volume histograms

Analyses of dose–volume histograms of patients' PTVs (Fig. 5) for the two groups (SSIMRT and TOMO) showed the following results: the mean dose maximum (Dmax) of the prescribed dose in the PTV prostate was 107.8% (standard error: 0.389) in the SSIMRT group and 104.3% (standard error: 0.415) in the TOMO group. The difference was significant ($P \le 0.05$). The mean volume (V) of the prostate PTV that received a dose more than 102% of the prescribed dose ($D > 102\%$) was 30.2% (standard error: 2.49; range: 8–47%) in the SSIMRT group and 4.57% (standard error: 0.61; range: 1–9%) in the TOMO group. This difference was also significant ($P \le 0.05$).

DISCUSSION

The method used for *in vivo* measurement of dose distribution within a patients's lymphocytes by detecting gamma-H2AX foci (and the potential limitations of this method) have been discussed earlier [2], whereas subsequent articles [6, 19–28] have considered what determines the presence of the lymphocytes in body tissue as a result of their kinetics—i.e. circulation, migration and adhesion to vessel walls.

Salk *et al*. have discussed these circumstances in detail previously [6]. In in-field capillaries, the speed of lymphocytes is slower; thus they receive a higher radiation dose than do the fast-moving lymphocytes in larger vessels. Differences in the mean number of gamma-H2XA foci in lymphocytes after dose exposure depend on the irradiated target sites, e.g. brain or thorax. The target site was not a variable parameter in our study. We compared TOMO and SSIMRT only for the treatment of prostate cancer. The PTV volume included blood vessels/rami of the arteria iliaca interna, which were reproducible and comparable in both patient groups.

Attention also must be paid to repair kinetics and the withdrawal of gamma-H2AX foci, which makes it necessary to stop cell metabolism after a certain duration post-irradiation. In this context, we fixed all cells 2 h after irradiation (*in vivo* and *in vitro*) to allow comparability between samples.

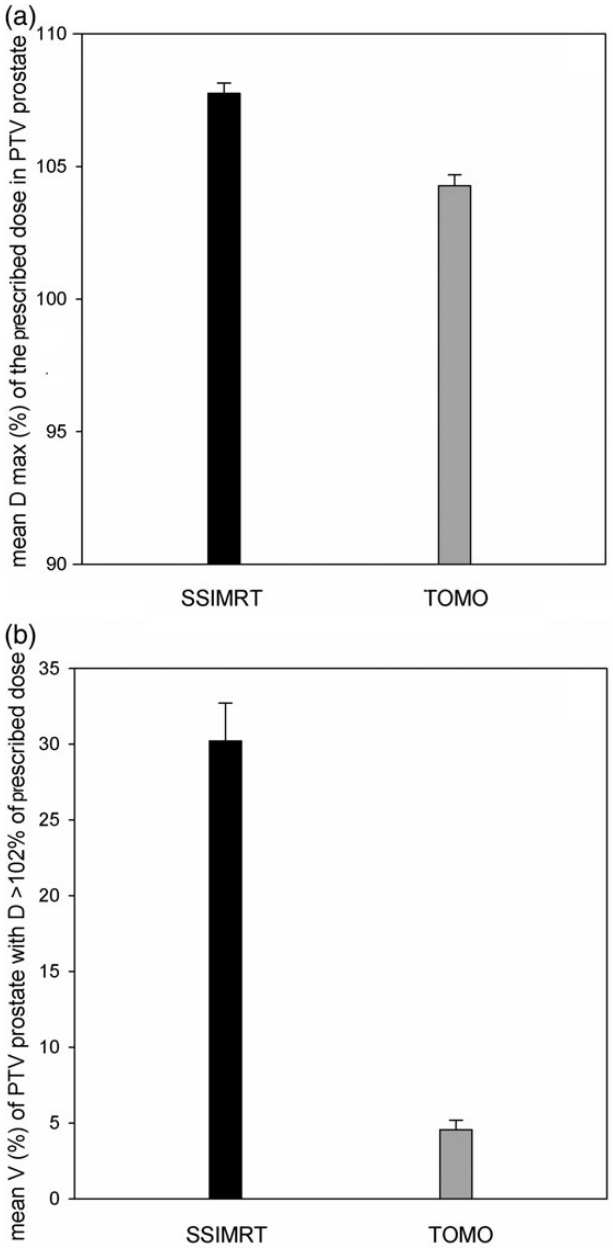

Fig. 5. Analyses of dose–volume histograms (DVH) of patients' PTV prostate of the SSIMRT and the TOMO group (20 patients each): (**a**) mean relative dose maximum (D max) of the prescribed dose in the PTV prostate, and (**b**) mean relative volume (V) of PTV prostate that received dose more than 102% of the prescribed dose (D > 102%). Standard errors are shown.

Considering the physical parameters of the two groups (Table 2), the dose rate (Gy/min) appears to be a different factor. In TOMO (8.7 Gy/min), the dose rate is 4.35-fold higher than in SSIMRT (2 Gy/min). This results in more inhomogeneity of the dose rate in a patients's irradiated volume in the TOMO group and may potentially produce a higher fraction of lymphocytes with low-dose exposure.

It cannot be ruled out that differences in dose rates can have distinct effects on the induction and withdrawal of gamma-H2AX foci. Speculatively, lower dose rates may result in slower gamma-H2AX foci withdrawal during repair, with potentially higher gamma-H2AX foci counts in the SSIMRT group. Conversely, higher dose rates may result in increased gamma-H2AX foci induction, with the same effect for the TOMO group. To date, it has only been described that a reduction of the dose rate from 2 Gy/min to 0.07 Gy/min (a factor of 30) produces no difference in the number of residual gamma-H2AX foci at 24 h after irradiation (2 Gy) [29]. However, reduction of the dose rate from 2 Gy/min to 0.07 Gy/min results in a slight but significant increase in clonogenic cell survival [29, 30]. Considering these results, it could be suggested that the difference in the dose rates of the two radiation techniques does not essentially influence the different results of the two groups (SSIMRT and TOMO) with respect to the distribution of gamma-H2AX foci in lymphocytes. But it has to be mentioned that data about this issue is rare in the literature.

At first, it is surprising that only SSIMRT appears to deliver >100% of the peak dose to some lymphocytes. Doses >100% of the applied dose were expected in the inner PTV of the prostate gland. The expected number of detected lymphocytes with doses >100% of the described dose is per se very small. The median dose of 2.17 Gy was prescribed to the PTV in both groups. Helical IMRT (tomotherapy) reached a significantly higher conformity in dose distribution than SSIMRT during radiotherapy for prostate cancer [31]. The corresponding DVH data of our study indicate that mean maximum doses and the percentage of the PTV with a dose >102% of the prescribed dose were significant higher in the SSIMRT group than in the TOMO group (see Fig. 5). Considering this, the difference in dose distribution of relative dose >100% in the patients' lymphocytes was more understandable.

Physical phantom measurements investigating the peripheral doses for different IMRT techniques published previously should also be considered in explaining the significantly smaller fraction of lymphocytes with low-dose exposure in the TOMO group.

The horizontal peripheral dose distribution in the lower dose range in SSIMRT is more heterogeneous than in TOMO. An influence on our results cannot be excluded, but it is difficult to define a conclusive relationship.

Recently, it was shown that for small PTVs (295 cm^3) in the horizontal direction, TOMO shows a slightly increased relative peripheral dose (RPD)—up to 0.8% compared with SSIMRT in a distance range of 15–20 cm around the central axis. For substantially larger volumes (2356 and 7952 cm^3), TOMO shows a distinct relative increase in horizontal RPD compared with SSIMRT [32].

In the same experimental setting, the RPD does not differ in SSIMRT compared with TOMO for small (295 cm^3) and

medium PTVs (2356 cm^3) in the vertical direction from the isocenter (measured distance ≤ 16 cm) [28]. The prostate PTV of all treated patients averaged 167.2 cm^3 in our study. Thus, we detected the dose distribution in lymphocytes of the whole body, requiring the consideration of the vertical peripheral dose.

It is believed that the vertical RPD in the whole body (out of the directly treated volume) is composed of sideways Compton-scattering from the irradiated volume and of radiation components of the linear accelerator (transmission and scatter doses of the machine-head and accelerator) [32–35]. Compton-scattering from the irradiated PTV depends on the photon energy and the size of the PTV [32]. The PTV and the total body volume were not significantly different between the two groups. The photon energy used in both groups was 6 MV.

However, it was shown by physical phantom measurements that the second important component of the RPD, which depends on leakage and shielding of the linear accelerator, is up to two-thirds lower in the Tomotherapy-HiArt system than in a Siemens linac [32, 34].

This linac-dependent component is relatively more important in the patient's distant periphery. In particular, the geometric construction of the linac (flattening filter, target and accelerator) may play a substantial role [32, 34]. In this context, results from Syme *et al*. (2009) [36] are notable. They reported that scattered radiation with lower energies may be more effective in inducing gamma-H2AX foci in human fibroblasts compared with open-beam radiation. At 2 Gy, the difference is up to 20%, whereas a scattering dose was applied at a lower dose rate.

Compared with the Siemens/Oncor system, the Tomotherapy-HiART system does not have a flattening filter, and the accelerator is located vertical to the longitudinal axis of the patient (in the Siemens/Oncor parallel). Previous results can shed light on this: the low-dose exposure in patients' lymphocytes and the mean number of gamma-H2AX foci per nucleus were not significantly different between 3D-conformal and SSIMRT techniques in radiotherapy of the prostate region, when both techniques were performed with the same linear accelerator (Siemens/Oncor) [2].

Considering the whole body volume, the Tomotherapy-HiArt system could perform lower vertical RPD compared with the Siemens/Oncor system. In our setting, the relationship of the PTV to body volume averaged 167 cm^3 to 86 000 cm^3, or 1:515. Therefore, the absolute number of lymphocytes exposed to vertical RPD is relatively higher than the lymphocytes exposed to horizontal RPD, apart from the consideration of the lymphocytes' movement.

This has been confirmed by experimental phantom measurements by Bennett *et al*. [37]. They compared the Tomotherapy-HiArt system with a classical linear accelerator in relation to the peripheral doses in an anthropomorphic whole-body phantom in IMRT for head and neck tumors. Within 2.5 cm (one TOMO field width) superior and inferior to the field edges, the normal tissue dose was significantly lower using a classic linear accelerator. However, beyond 2.5 cm in the vertical direction, the TOMO normal tissue dose was an average of 52% lower. From this, they calculated a probability of secondary malignancy of 5.88% for the classical linear accelerator and 4.08% for the TOMO in their set-up [37].

In our set-up, we also measured the dose distribution in lymphocytes for the whole body.

The significantly decreased fraction of lymphocytes with low-dose exposure during TOMO compared with SSIMRT can be observed in the context of the results discussed above. It is also notable that Bennett's results correspond with our findings, even though the PTV of head and neck tumors is substantially larger than the PTV in prostate cancer.

Our *in vivo* results confirm in principle the measurement of peripheral doses in the anthropomorphic phantom [37]. The influences of the different radiation techniques on secondary malignancy rates could be explored through retrospective analyses in the future.

The results of our study are only representative of small PTVs (in our study, up to ca. 350 cm^3). Whether our results are transferable to cases of larger volumes is uncertain. Further investigations with larger volumes are necessary.

The results of Bennett *et al*. [37] support the thesis that whole-body low-dose exposure is also lower in the case of a larger PTV (e.g. head and neck tumors) during TOMO than in step-and-shoot IMRT.

With respect to its limits, the *in vivo* method of measuring the dose distribution by gamma-H2AX foci in lymphocytes and creating a dose–lymphocyte histogram can help to estimate differences in whole body dosimetry between different irradiation techniques.

CONCLUSION

In summary, TOMO causes low-dose exposure of a smaller fraction of a patients's lymphocytes relative to the entire body compared with the step-and-shoot-IMRT in radiotherapy of the prostate gland. Differences in the constructional buildup of the different linear-accelerator systems, e.g. a flattening filter, may be the cause of this variation.

FUNDING

The authors all confirm that there has been no funding to support the research for this paper. Funding to pay the Open Access publication charges for this article was provided by Dr med. F.Z.

REFERENCES

1. Wiezorek T, Brachwitz T, Georg D *et al*. Rotational IMRT techniques compared to fixed gantry IMRT and tomotherapy: multi-institutional planning study for head-and-neck cases. *Radiat Oncol* 2011;**6**:20.
2. Zwicker F, Swartman B, Sterzing F *et al*. Biological *in-vivo* measurement of dose distribution in patients' lymphocytes by gamma-H2AX immunofluorescence staining: 3D conformal- vs. step-and-shoot IMRT of the prostate gland. *Radiat Oncol* 2011;**6**:62.
3. Löbrich M, Rief N, Kühne M *et al*. *In vivo* formation and repair of DNA double-strand breaks after computed tomography examinations. *Proc Natl Acad Sci U S A* 2005;**102**: 8984–9.
4. Rogakou EP, Pilch DR, Orr AH *et al*. DNA double-stranded breaks induce histone H2AX phosphorylation on serine 139. *J Biol Chem* 1998;**273**:5858–68.
5. Rogakou EP, Boon C, Redon C *et al*. Megabase chromatin domains involved in DNA double-strand breaks *in vivo*. *J Cell Biol* 1999;**146**:905–16.
6. Sak A, Grehl S, Erichsen P *et al*. Gamma-H2AX foci formation in peripheral blood lymphocytes of tumor patients after local radiotherapy to different sites of the body: dependence on the dose-distribution, irradiated site and time from start of treatment. *Int J Radiat Biol* 2007;**83**:639–52.
7. Rothkamm K, Löbrich M. Evidence for a lack of DNA double-strand break repair in human cells exposed to very low x-ray doses. *Proc Natl Acad Sci U S A* 2003;**100**:5057–62.
8. Méndez-Acuña L, Di Tomaso MV, Palitti F *et al*. Histone post-translational modifications in DNA damage response. *Cytogenet Genome Res* 2010;**128**:28–36.
9. Zwicker F, Ebert M, Huber PE *et al*. A specific inhibitor of protein kinase CK2 delays gamma-H2AX foci removal and reduces clonogenic survival of irradiated mammalian cells. *Radiat Oncol* 2011;**6**:15.
10. Prokic V, Geinitz H, Kneschaurek *et al*. Reduction of dosimetric impact of intrafractional prostate motion during helical tomotherapy. *Strahlenther Onkol* 2012 **188**:404–9.
11. Jereczek-Fossa BA, Pobbiati C, Santoro L *et al*. Prostate positioning using cone-beam computer tomography based on manual soft-tissue registration: interobserver agreement between radiation oncologists and therapists. *Strahlenther Onkol* 2013;**190**:81–87.
12. Manabe Y, Shibamoto Y, Sugie C *et al*. Toxicity and efficacy of three dose-fractionation regimens of intensity-modulated radiation therapy for localized prostate cancer. *J Radiat Res* 2014;**55**:494–501.
13. Shinohara N, Maruyama S, Shimizu S *et al*. Longitudinal comparison of quality of life after real-time tumor-tracking intensity-modulated radiation therapy and radical prostatectomy in patients with localized prostate cancer. *J Radiat Res* 2013;**54**:1095–101.
14. Krause S, Beck S, Schramm O *et al*. Tomotherapy radiosurgery for arteriovenous malformations – current possibilities and future options with helical tomotherapy dynamic jaws? *Technol Cancer Res Treat* 2013;**12**:421–8.
15. Welsh JS, Patel RR, Ritter MA *et al*. Helical tomotherapy: an innovative technology and approach to radiation therapy. *Technol Cancer Res Treat* 2002;**1**:311–6.
16. Shepard DM, Olivera GH, Reckwerdt PJ *et al*. Iterative approaches to dose optimization in tomotherapy. *Phys Med Biol* 2000;**45**:69–90.
17. Schlegel W, Kneschaurek P. Inverse radiotherapy planning. *Strahlenther Onkol* 1999;**175**:197–207.
18. Kuefner MA, Grudzenski S, Schwab SA *et al*. X-ray-induced DNA double-strand breaks after angiographic examinations of different anatomic regions. *Röfo* 2009;**181**:374–80.
19. Kuefner MA, Grudzenski S, Hamann J *et al*. Effect of CT scan protocols on x-ray-induced DNA double strand breaks in blood lymphocytes of patients undergoing coronary CT angiography. *Eur Radiol* 2010;**20**:2917–24.
20. MacPhail SH, Banáth JP, Yu TY *et al*. Expression of phosphorylated histone H2AX in cultured cell lines following exposure to X-rays. *Int J Radiat Biol* 2003;**79**:351–8.
21. Banáth JP, Macphail SH, Olive PL *et al*. Radiation sensitivity, H2AX phosphorylation, and kinetics of repair of DNA strand breaks in irradiated cervical cancer cell lines. *Cancer Res* 2004;**64**:7144–9.
22. Modesti M, Kanaar R. DNA repair: spot(light)s on chromatin. *Curr Biol* 2001;**11**:229–32.
23. Olive PL, Banáth JP. Phosphorylation of histone H2AX as a measure of radiosensitivity. *Int J Radiat Oncol Biol Phys* 2004;**58**:331–5.
24. Olive PL, Banáth JP, Sinnott LT. Phosphorylated histone H2AX in spheroids, tumors, and tissues of mice exposed to etoposide and 3-amino-1,2,4-benzotriazine-1,3-dioxide. *Cancer Res* 2004;**64**:5363–9.
25. Andrievski A, Wilkins RC. The response of gamma-H2AX in human lymphocytes and lymphocytes subsets measured in whole blood cultures. *Int J Radiat Biol* 2009;**85**:369–76.
26. Rothkamm K, Balroop S, Shekhdar J *et al*. Leukocyte DNA damage after multi-detector row CT: a quantitative biomarker of low-level radiation exposure. *Radiology* 2007;**242**: 244–51.
27. Bells L, Werbrouck J, Thierens H. Dose response and repair kinetics of gamma-H2AX foci induced by *in vitro* irradiation of whole blood and T-lymphocytes with X- and gamma-radiation. *Int J Radiat Biol* 2010;**86**:760–8.
28. Jucha A, Wegierek-Ciuk A, Koza Z *et al*. Foci-Counter: a freely available PC programme for quantitative and qualitative analysis of gamma-H2AX foci. *Mutat Res* 2010;**696**:16–20.
29. Moiseenko V, Banáth JP, Duzenli C *et al*. Effect of prolonging radiation delivery time on retention of gammaH2AX. *Radiat Oncol* 2008;**3**:18.
30. Sterzing F, Münter MW, Schäfer M *et al*. Radiobiological investigation of dose-rate effects in intensity-modulated radiation therapy. *Strahlenther Onkol* 2005;**181**:42–8.
31. Wolff D, Stieler F, Welzel G *et al*. Volumetric modulated arc therapy (VMAT) vs. serial tomotherapy, step-and-shoot IMRT and 3D-conformal RT for treatment of prostate cancer. *Radiother Oncol* 2009;**93**:226–33.
32. Wiezorek T, Schwahofer A, Schubert K. The influence of different IMRT techniques on the peripheral dose: a comparison

between sMLM-IMRT and helical tomotherapy. *Strahlenther Onkol* 2009;**185**:696–702.
33. Wiezorek T, Voigt A, Metzger N *et al*. Experimental determination of peripheral doses for different IMRT techniques delivered by a Siemens linac accelerator. *Strahlenther Onkol* 2008;**184**:73–9.
34. Wiezorek T, Georg D, Schwedas M *et al*. Experimental determination of peripheral photon dose components for different IMRT techniques and linear accelerators. *Z Med Phys* 2009;**19**:120–8.
35. Chofor N, Harder D, Willborn KC *et al*. Internal scatter, the unavoidable major component of the peripheral dose in photon-beam radiotherapy. *Phys Med Biol* 2012;**57**:1733–43.
36. Syme A, Kirkby C, Mirzayans R *et al*. Relative biological damage and electron fluence in and out of a 6 MV photon field. *Phys Med Biol* 2009;**54**:6623–33.
37. Bennett BR, Lamba MA, Elson HR. Analysis of peripheral doses for base of tongue treatment by linear accelerator and helical TomoTherapy IMRT. *J Appl Clin Med Phys* 2010;**11**: 3136.